5th International Conference on Experimental Fluid Mechanics ICEFM 2018 Munich
Munich, Germany, July 2-4, 2018

# PIV-based load estimation in three-dimensional flow

**Jeffrey McClure*, Serhiy Yarusevych**

University of Waterloo, Department of Mechanical and Mechatronics Engineering, Waterloo, Canada

* jejmcclu@uwaterloo.ca

## Abstract

The application of momentum balance over a planar control volume is ubiquitous in experimental fluid mechanics. The classical formulation relies on an assumption of two-dimensional flow which is routinely violated in turbulent or transitional flows. The additional terms required for an exact momentum balance are evaluated herein. It is shown that the divergence-free condition on the velocity field in incompressible flow may be invoked to account for a subset of the additional three-dimensional terms, enabling an increase in accuracy. The derived formulation is verified using instantaneous and mean planar control volume load estimations on direct numerical simulation and experimental particle image velocimetry data for flow over a cylinder in a turbulent wake regime. The main result is the demonstration of the significance of the area integrals involving out-of-plane velocity and gradients on the instantaneous load estimates. The findings highlight a possible cause of difficulties in obtaining consistent estimates of instantaneous sectional loads for three-dimensional flows using control volume methods, and provide guidelines for minimizing methodological or user dependant errors in experiment.

## 1 Introduction

The measurements of flow-induced loading is a fundamental component of aerodynamic testing, as the reliable estimation of structural loads is of primary interest for engineering design. There are three common approaches to measuring loads, namely, (i) full-body, direct measurements with a force balance, (ii) integration of surface stresses (i.e., pressure and/or wall shear stress), and (iii) analysis of field measurements, e.g., control volume (CV)-based methods, (Unal et al., 1997a; van Dam, 1999; Rival and van Oudheusden, 2017). Each approach can offer an advantage in simplicity or accuracy depending on the experimental context, and each poses specific challenges and limitations. The present study is focused on load estimation from CV analysis.

A large number of formulations are possible based on classical CV analysis. For instantaneous loading estimates, time-resolved velocimetry is generally required in order to evaluated the unsteady terms within the volume. Analytically, the simplest method is the classical integral momentum balance, (Unal et al., 1997a), where the pressure term is typically estimated from pressure fields obtained using measured velocity fields (e.g.,(Unal et al., 1997a; van Oudheusden, 2013)). If near-wall velocity data is missing or significantly erroneous and the flow is incompressible, a derivative-moment transform may be applied to the unsteady volume integral term to transform it into a contour integral (Wu et al., 2005); however, the resulting unsteady term demands increased spatial resolution to maintain accuracy (Mohebbian and Rival, 2012). These two formulations for instantaneous load estimation may be widely grouped as integral momentum equation approaches, and have been applied in numerous studies (Unal et al., 1997b; van Oudheusden et al., 2006, 2007; Kurtulus et al., 2007; Spedding and Hedenström, 2009; David et al., 2009; Ragni et al., 2012; Kotsonis et al., 2011; Tronchin et al., 2015; Villegas and Diez, 2014; Gharali and Johnson, 2014). Alternatively, loading estimates may be derived from the concept of hydrodynamic impulse (Lin and Rockwell, 1996; Poelma et al., 2006), which eliminates the need for pressure field estimates at the expense of vorticity field estimates (Saffman, 1992; Noca et al., 1999a; Wu et al., 2006; Kriegseis and Rival, 2014; DeVoria et al., 2013; Rival and van Oudheusden, 2017; Guissart et al., 2017; Graham and Babinsky, 2017; Limacher et al., 2018). Recently, another alternative to the classical integral momentum balance has been developed which utilizes the concept of the Lagrangian drift volume to estimate unsteady loads for added mass dominated flows (McPhaden and Rival, 2018).

Despite the wide-spread use of CV-based methods for load estimation, concrete experimental methodology guidelines remain largely unresolved. As a consequence, the source of bias and random errors in load

estimations is not always clear (van Dam, 1999; Bohl and Koochesfahani, 2009; Kurtulus et al., 2007; van Oudheusden et al., 2007). In contrast, verification studies for CV-based instantaneous and mean load estimations from *two-dimensional* direct numerical simulations (DNS) give close agreement with solver values (David et al., 2009; Noca et al., 1999b; Mohebbian and Rival, 2012). In the present study, a general CV formulation for three-dimensional flows is considered and the effect of flow three-dimensionality is investigated. The exact formulation for sectional load estimation on a planar CV is derived, and the dependency of the associated instantaneous and mean load estimates on flow three-dimensionality is deduced for a synthetic PIV data set sampled from DNS data and a matching experimental PIV experiment for cross-flow over a circular cylinder.

## 2 Conservation of linear momentum for a planar CV

The conservation of linear momentum over $V \subset \mathbb{R}^3$ for a stationary, non-deforming CV in a single-phase flow with velocity $\boldsymbol{u}(\boldsymbol{x},t) = (u(\boldsymbol{x},t), v(\boldsymbol{x},t), w(\boldsymbol{x},t))$, density $\rho(\boldsymbol{x},t)$ and pressure $p(\boldsymbol{x},t)$ fields is:

$$\sum \boldsymbol{F}_{CV} = \frac{d}{dt}\left(\iiint_V \rho \boldsymbol{u} dV\right) + \iint_\Omega \rho \boldsymbol{u}(\boldsymbol{u}\cdot d\boldsymbol{A}) \tag{1}$$

where $V$ denotes the fluid volume and $\Omega$ denotes the boundaries of $V$. For the case of a single stationary body inside the CV, the force vector $\boldsymbol{F} = (F_x(t), F_y(t), F_z(t))$ acting on the body is:

$$\boldsymbol{F} = -\frac{d}{dt}\left(\iiint_V \rho \boldsymbol{u} dV\right) - \iint_S \rho \boldsymbol{u}(\boldsymbol{u}\cdot\boldsymbol{n}) dA - \iint_S p\boldsymbol{n} dA + \iint_S (\boldsymbol{\tau}\cdot\boldsymbol{n}) dA - \iiint_V \rho \boldsymbol{f} dV \tag{2}$$

where $\boldsymbol{f}$ denotes an arbitrary body force, $\boldsymbol{\tau}$ denotes the viscous stress tensor field, and $S$ now denotes the outer boundary of the doubly-connected domain, $V$.

For the momentum balance on a two-dimensional plane, it does not suffice to only evaluate equation 2 with the projected two-dimensional flow. Instead, area integrals of the three-dimensional terms are necessary for momentum conservation. This implies that volumetric measurements surrounding an immersed body are required for sectional load estimation (Equation 3), which may not be feasible in practice. However, for planar, two-component measurement configurations in incompressible flow, the three-dimensional terms can be made partially tractable through the application of the divergence-free constraint on the velocity field (Equation 4). To benchmark the accuracy of different possible measurement methodologies, the following three formulations are compared in the present study.

$$\boldsymbol{F_S} = -\frac{d}{dt}\left(\iint_S \rho \boldsymbol{u} dA\right) - \oint_l \rho \boldsymbol{u}(\boldsymbol{u}\cdot\boldsymbol{n}) dl - \iint_S \left(\rho w \frac{\partial \boldsymbol{u}}{\partial z} + \rho \boldsymbol{u}\frac{\partial w}{\partial z}\right) dA - \oint_l p\boldsymbol{n} dl + \iint_S \mu\left(\frac{\partial^2 \boldsymbol{u}}{\partial z^2} + \mu\nabla\left(\frac{\partial w}{\partial z}\right)\right) dA \tag{3}$$

$$\boldsymbol{F_S} = -\frac{d}{dt}\left(\iint_S \rho \boldsymbol{u} dA\right) - \oint_l \rho \boldsymbol{u}(\boldsymbol{u}\cdot\boldsymbol{n}) dl + \iint_S \rho \boldsymbol{u}\left(\nabla_{xy}\cdot\boldsymbol{u}\right) dA - \oint_l p\boldsymbol{n} dl - \iint_S \mu\nabla\left(\nabla_{xy}\cdot\boldsymbol{u}\right) dA \tag{4}$$

$$\boldsymbol{F_S} = -\frac{d}{dt}\left(\iint_S \rho \boldsymbol{u} dA\right) - \oint_l \rho \boldsymbol{u}(\boldsymbol{u}\cdot\boldsymbol{n}) dl - \oint_l p\boldsymbol{n} dl \tag{5}$$

Equations (3) and (4) are referred to as the exact and approximate formulations, respectively, and represent volumetric measurement and planar measurement in incompressible flow. Equation (5) is representative of the classical planar CV formulation.

## 3 Test Cases

Two data-sets were employed of flow over a circular cylinder in a turbulent vortex shedding regime, namely, three-dimensional DNS results at $Re = 1575$, and experimental, planar, two-component data for $Re = 1900$.

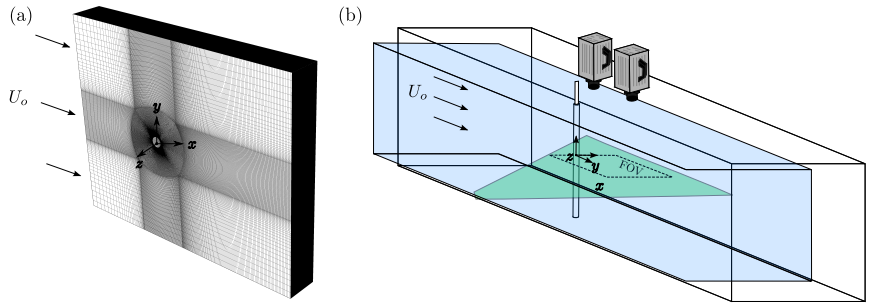


Figure 1: (a) DNS computational mesh configuration and (b) experimental PIV measurement configuration.

Details of the DNS are included in McClure and Yarusevych (2017b) and the computational mesh is shown in Figure 1a. The DNS data were sampled in two ways to facilitate the analysis. First, a fully three-dimensional data set was sampled, where both pressure and velocity fields from the DNS results were directly interpolated onto a three-dimensional Cartesian grid with spatial resolution $\Delta x/D = 0.01$ and temporal resolution $f_{acq}/f_S = 217.4$, where $D$ and $f_S$ are the cylinder diameter and the vortex shedding frequency, respectively. Second, a noisy planar data set was constructed, where the velocity data were interpolated onto a two-dimensional grid with spatial resolution $\Delta x/D = 0.03$ and temporal resolution $f_{acq}/f_S = 27.3$, and synthetic errors were added to the interpolated velocity fields according to the two parameter model presented in McClure and Yarusevych (2017a). The model prescribed error proportional to the local norm of the velocity gradient tensor, up to a maximum standard deviation of $0.25U_0$, along with flow independent error, with a standard deviation of $0.036U_0$. The errors were generated to be correlated locally in space, modelling the effect of PIV interrogation window overlap of 75% (Azijli and Dwight, 2015).

The experimental PIV measurements were obtained in the water flume facility at the University of Waterloo (figure 1b) on a 25.4$mm$ inch diameter acrylic cylinder model at $Re = 1900$. The PIV system comprised of a single $1024 \times 1024px$ Photron SA4 camera, equipped with a $50mm$ Nikkor lens with the numerical aperture set to $f/5.6$, and a Photonics high repetition rate Nd:YLF laser. The flow was seeded with $10\mu m$ diameter hollow glass spheres, with specific gravity of 1.05. The particle images were acquired in single-frame mode at $f_{acq} = 100Hz$ ($147f_S$), and were processed in DaVis 8.4 using an iterative, multi-grid cross-correlation algorithm with window deformation. The final interrogation window size was $16 \times 16$ pixels, overlapped by 75%, and yielded a vector pitch of approximately $\Delta x/D = 0.03$.

The Poisson equation (6) was employed to estimate the pressure fields (e.g., Gurka et al., 1999) from both the PIV and simulated planar velocity fields with noise extracted from the DNS data set.

$$\left.\begin{aligned} \nabla^2 p &= \nabla \cdot \left( -\rho \frac{D\boldsymbol{u}}{Dt} + \mu \nabla^2 \boldsymbol{u} \right) \quad \text{in} \quad S, \\ \nabla p \cdot \boldsymbol{n} &= \left( -\rho \frac{D\boldsymbol{u}}{Dt} + \mu \nabla^2 \boldsymbol{u} \right) \cdot \boldsymbol{n} \quad \text{on} \quad \Gamma_i, \\ p &= \frac{1}{2}\rho U_0^2 - \frac{1}{2}\rho \left( \overline{\boldsymbol{u}} \cdot \overline{\boldsymbol{u}} + \boldsymbol{u}' \cdot \boldsymbol{u}' \right) \quad \text{on} \quad \Gamma_j, \end{aligned}\right\} \tag{6}$$

The source terms and pressure gradients in equation 6 were evaluated with a central difference approximation. Neumann-type boundary conditions were prescribed at the outflow domain boundary and the cylinder surface, and an extended form of Bernoulli's equation (de Kat and van Oudheusden, 2012) was used on the inflow and top/bottom side boundaries, where flow was approximately steady and irrotational. The relative spatial resolution of the PIV data is $\Delta x/\lambda_x = 13.6$ where $\lambda_x$ is twice the shear layer thickness, and the PIV data were down sampled to a relative temporal resolution of $f_{acq}/f_S = 13.4$. These resolutions coincide with optimal ranges identified in McClure and Yarusevych (2017b) that minimize the propagation of random and truncation errors to the pressure solution without the use of low-pass filtering techniques.

# 4 Results

Figures 2(a) presents instantaneous snapshots of the pressure field obtained directly from DNS (figure 2a),

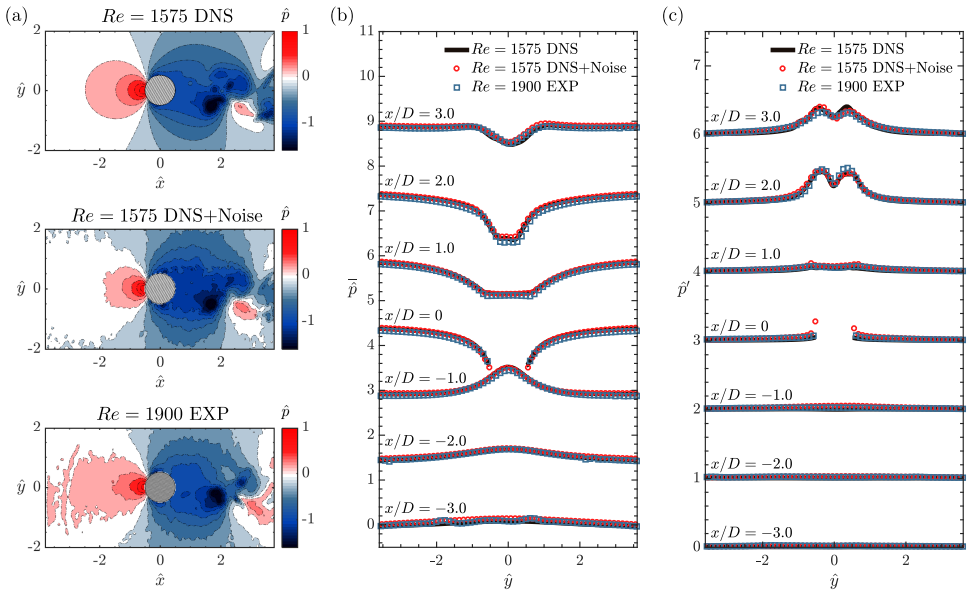


Figure 2: (a) Instantaneous pressure fields $\hat{p} = 2p/\rho U_0^2$ for direct interpolation of the DNS solver pressure, Poisson solution on the down sampled DNS velocity fields with synthetic noise, and Poisson solution on the PIV velocity fields. Transverse profiles of (b) mean pressure, and (c) RMS of the pressure fluctuations at multiple streamwise locations.

the Poisson solution on the noisy planar DNS (figure 2b), and the Poisson solution on the experimental planar PIV data (figure 2c). The instantaneous fields indicate qualitative similarity between the cases, and highlight that the synthetic noisy DNS data serves as a reasonable approximation of experiment. Figures 2(b) and 2(c) plot transverse profiles of the mean and RMS pressure at several streamwise locations. The results show a good agreement between the three cases, indicating the minor *Re* difference does not have a significant effect on the comparison between the DNS and experimental data. Deviations in the estimated pressure relative to the DNS solver pressure are attributed primarily to omitted three-dimensional terms in the Poisson source term (Violato et al., 2011; Ghaemi et al., 2012; McClure and Yarusevych, 2017b), in regions of pronounced three-dimensional flow ($\hat{x} = x/D > 1.5$). As well, random errors inflate the pressure RMS statistic near the cylinder wall boundary, due to the sensitivity of the Neumann boundary condition. The errors in the estimated pressure field are higher near the cylinder wall boundary for the noisy planar DNS data than the errors encountered in experiment (figure 2b). This is due to the synthetic error model, which concentrates the synthetic PIV errors in high gradient near-wall regions. The prescribed maximum standard deviation of the errors of $0.25U_0$ in the near-wall region over predict the error actually realized in the current experiment.

Equations (3)-(5) predict the sensitivity of the approximate (4) and classical (5) momentum equation to flow three-dimensionality. Analysis of the three-dimensional velocity statistics from DNS indicates the onset of significant three-dimensionality beyond $\hat{x} > 1.5$. Hence, to clearly demonstrate the three-dimensional effect on instantaneous loading estimates, figure 3 presents the time history of the sectional drag and lift coefficients obtained by applying the exact (3), approximate (4), and classical (5) formulations to the direct DNS data set for two different CV sizes. The first CV (figure 3a, $L_{CV} = 4.0$), includes regions of significant three-dimensional flow, in contrast to the second CV (figure 3b, $L_{CV} = 1.9$), which includes only regions of predominantly two-dimensional flow. Here, $L_{CV}$ is the side length of the square CV, which is centred at the cylinder centre. The results demonstrate that the exact CV formulation (3) is the correct linear momentum conservation law for the planar CV, with force estimates matching the surface integrated results from the DNS solver for both CVs. On the other hand, when three-dimensional flow regions are present within the CV (figure 3a), simplified formulations (4) and (5) can lead to significant errors in instantaneous force estimates. Specifically, the classical formulation (5) yields significantly erroneous instantaneous results for both the lift and drag forces, and while the use of the approximate form (4) yields some improvement over the classical formulation, significant instantaneous deviations remain. As expected, when the CV is constructed to bound minimal flow three-dimensionality (figure 3b), the approximate and classical formulations approach the

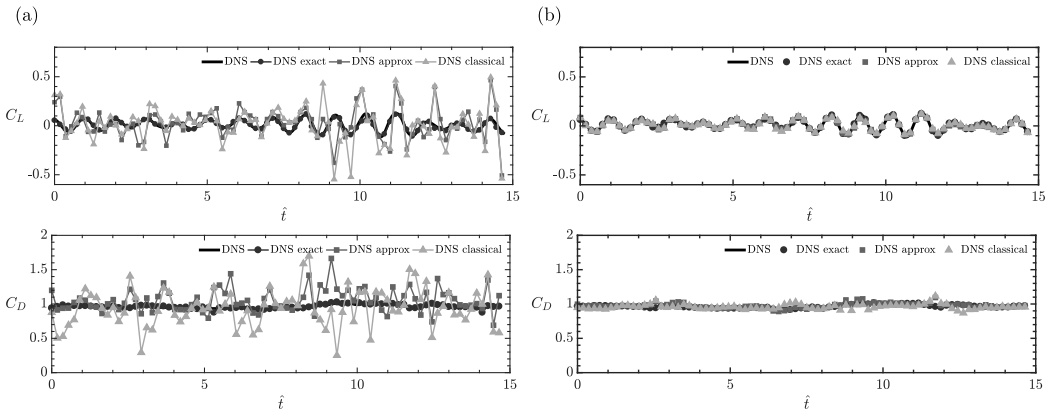


Figure 3: Time evolution of CV sectional drag coefficient $C_D(t) = 2F_x(t)/\rho U_0^2 D$ and sectional lift coefficient $C_L = 2F_y(t)/\rho U_0^2 D$ estimates using equations (3), (4), and (5) on the DNS data compared to surface integrated loads from the DNS solver: (a) corresponds to $L_{CV} = 1.9$, and (b) corresponds to $L_{CV} = 4.0$.

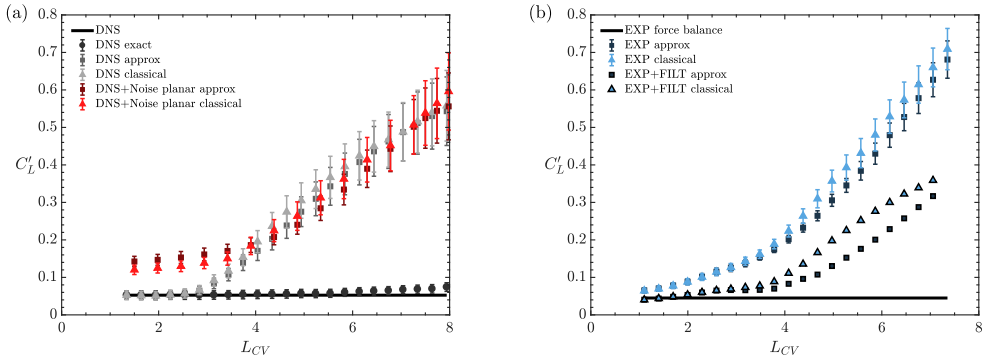


Figure 4: RMS lift forces evaluated using equations (3), (4), and (5) for variable CV size ($L_{CV}$) for (a) direct DNS and noisy, planar DNS at $Re = 1575$ and (b) PIV experiment at $Re = 1900$.

DNS reference data as well. Note that the pressure term for the direct data set used in figure 3 remains sampled from the exact DNS solver pressure, such that all deviations present are solely due to the three-dimensional momentum flux terms in equation (3) in this case.

To more comprehensively characterize and quantify the accuracy of the CV formulations in the presence of three-dimensional flow and experimental errors, the CV size ($L_{CV}$) is systematically varied, and loading estimates obtained by applying the different formulations to the test data sets are compiled. All estimates from DNS are compared to the surface integrated forces from the DNS solver, while all estimates from the PIV experiment are compared to sectional forces derived from force balance measurements and spanwise correlation measurements in the same facility (McClure and Yarusevych, 2016).

Figures 4(a) and 4(b) compare the results for the RMS lift statistics ($C'_L$) for DNS and experimental data, respectively. The results from the exact formulation based on three-dimensional DNS data match the direct force results. Furthermore, all formulations using the exact data exhibit close agreement to the DNS solver RMS lift if the CV size is small (figure 4a), but the approximate and classical formulations yield progressively increasing deviations in the RMS lift statistic when $L_{CV}$ starts to encompass three-dimensional flow regions, with errors reaching up to 1000% for the largest CVs. In the cases of the planar DNS and PIV data, which include errors in the velocity fields, the propagation of random error from the velocity fields through the CV formulation is also significant, even for small CV sizes. The influence of the random error on the instantaneous force estimates motivates the use of zero-phase temporal low-pass filtering for each term in the formulation for the estimations from the PIV data set (figure 4b). Here, a low-pass, equiripple finite-impulse response filter with a pass band at $1.5 f_S$ and a $60dB$ stop band at $15 f_S$ is employed, and the results in figure 4(b) show the improved accuracy of the estimates once the fluctuation energy at the vortex shedding frequency is isolated. Note that the high errors displayed here are due in part to the relatively

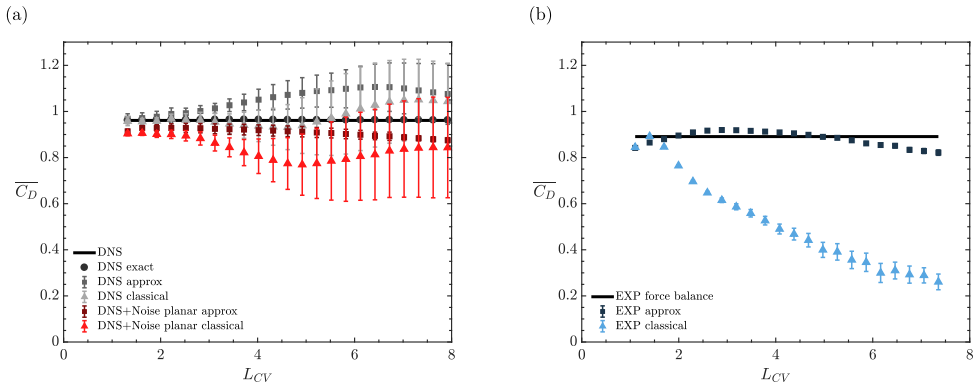


Figure 5: Mean drag forces evaluated using equations (3), (4), and (5) for variable CV size ($L_{CV}$) for (a) direct DNS and noisy, planar DNS at $Re = 1575$, and (b) PIV experiment at $Re = 1900$.

low magnitude of the fluctuating lift coefficient, where the lift force is determined through a cancellation of much larger magnitude transverse momentum terms and unsteady momentum terms for large CVs. Hence, for different flow cases, the three-dimensional terms may appear less significant simply due to their relative magnitude, such as in the case of moving bodies, where lift coefficients commonly reach up to 1.0-2.0.

Figure 5(a) plots estimates of mean drag for the three-dimensional and planar DNS data sets, while figure 5(b) plots mean drag estimates from the PIV experiment. In both the numerical and experimental data sets (figures 5a,b), the classical and approximate CV formulations show dependency of the mean drag on the CV size, while the exact formulation is insensitive to CV size and exhibits universal agreement with the DNS solver drag (figure 5a). The disagreement of the approximate and classical formulations with the DNS solver drag is primarily a matter of statistical convergence. In particular, the random errors induced by the three-dimensional terms are so significant relative to the mean drag ($> 100\%C_D$), that the estimate of the mean does not achieve a sufficient convergence over the time sample of DNS data, which is accounted for in the estimated error bars. For the noisy planar DNS data, the mean drag is underpredicted compared to the exact DNS data set, even for small CV sizes (figure 5a). This is ascribed to truncation error accumulation due to the lower spatial resolution employed. A similar trend is seen for the experimental case (figure 5b); however, the disparity between the mean drag estimates becomes more pronounced with increasing CV size compared to the numerical case. In the experimental case, the means are better converged due to a longer time sample compared to the DNS. Here, the disagreement with the force balance data suggests a high sensitivity of the CV force estimates to slight flow three-dimensionalities present in experiment.

# 5 Conclusion

Loading estimates based on the integral momentum equation over a planar CV are tested for their sensitivity to three-dimensional flow conditions for a cylinder wake flow. In comparison to the classical, two-dimensional formulation (5), the full three-dimensional formulation (3) includes area integrals involving the out-of-plane velocities and gradients associated with the out-of-plane momentum flux and viscous forces. The formulation is validated on a prototypical cylinder wake flow in a turbulent shedding regime using a combined analysis of DNS and experimental PIV data. The results reveal the significant implications flow three-dimensionality has on both instantaneous and mean sectional load estimation methodologies common in aerodynamic testing. Failure to account for the three-dimensional terms leads to instantaneous and mean errors on the order of 50%, and are shown to be the cause of loading estimates sensitivity to CV location. Invoking a divergence-free condition for incompressible flow allows the estimation of a subset of the expanded three-dimensional terms, yielding a minor increase in accuracy over the classical two-dimensional formulation for the test case considered. The cumulative results suggest that, when only planar velocity measurements are possible, it is best to strategically select a CV to avoid encompassing three-dimensional flow regions, employ temporal filtering to mitigate random error propagation, and use the approximate CV formulation (4) to enable instantaneous loading estimates with the highest precision. Regions of three-dimensional flow can be identified in planar measurement, for example, through a comparative analysis of the planar divergence statistics over the domain.

## Acknowledgements

The authors gratefully acknowledge the contribution of the Natural Science and Engineering Research Council (NSERC) to the funding of this research.

## References

Antonia RA and Rajagopalan S (1990) Determination of drag of a circular cylinder.. *AIAA Journal* 28:1833–1834

Azijli I and Dwight R (2015) Solenoidal filtering of volumetric velocity measurements using Gaussian process regression. *Exp Fluids* 56:198

Betz A (1925) A method for the direct determination of wing-section drag.. Technical Report 337. NACA Tech. Mem.

Bohl D and Koochesfahani M (2009) MTV measurements of the vortical field in the wake of an airfoil oscillating at high reduced frequency. *J Fluid Mech* 620:63–88

David L, Jardin T, and Farcy A (2009) On the non-intrusive evaluation of fluid forces with the momentum equation approach. *Meas Sci Technol* 9:095401

de Kat R and van Oudheusden B (2012) Instantaneous planar pressure determination from PIV in turbulent flow. *Exp Fluids* 52:1089–1106

DeVoria A, Zakery R, and Ringuette M (2013) On calculating forces from the flow field with application to experimental volume data. *J Fluid Mech* 749:297–319

Ghaemi S, Ragni D, and Scarano F (2012) PIV-based pressure fluctuations in the turbulent boundary layer. *Exp Fluids* 53:1823–1840

Gharali K and Johnson D (2014) PIV-based load investigation in dynamic stall for different reduced frequencies. *Exp Fluids* 55:1803

Graham aPFC WR and Babinsky H (2017) An impulse-based approach to estimating forces in unsteady flow. *J Fluid Mech* 815:60–76

Guissart A, Bernal L, Dimitriadis G, and Terrapon V (2017) PIV-based estimation of unsteady loads on a flat plate at high angle of attack using momentum equation approaches. *Exp Fluids* 58:53

Gurka R, Liberzon A, Hefetz D, Rubinstein D, and Shavit U (1999) Computation of pressure distribution using PIV velocity data. in *3rd Int. Workshop on Particle Image Velocimetry*. pages 671–676. Santa Barbara

Jones BM (1936) The measurement of profile drag by the pitot-traverse method.. Technical Report 1688. Air Ministry - Aeronautical Research Committe Reports and Memoranda

Kotsonis M, Ghaemi S, Veldhuis L, and Scarano F (2011) Measurement of the body force field of plasma actuators. *Journal of Physics D: Applied Physics* 44:045204

Kriegseis J and Rival D (2014) Vortex force decomposition in the tip region of impulsively-started flat plates. *J Fluid Mech* 756:758–770

Kurtulus D, Scarano F, and David L (2007) Unsteady aerodynamic forces estimation on a square cylinder by TR-PIV. *Exp Fluids* 42:185–196

Limacher E, Morton C, and Wood D (2018) Generalized derivation of the added-mass and circulatory forces for viscous flows. *Phys Rev Fluids* 3:014701

Lin J and Rockwell D (1996) Force identification by vorticity fields: techniques based on flow imaging. *J Fluids Stuct* 10:663–668

McClure J and Yarusevych S (2016) Vortex shedding and structural loading characteristics of finned cylinders. *J Fluids Struct* 10:100–101

McClure J and Yarusevych S (2017a) Instantaneous PIV/PTV-based pressure gradient estimation: a framework for error analysis and correction. *Exp Fluids* 58:92

McClure J and Yarusevych S (2017b) Optimization of planar PIV-based pressure estimates in laminar and turbulent wakes. *Exp Fluids* 58:62

McPhaden C and Rival D (2018) Unsteady force estimation using a Lagrangian drift-volume approach. *Exp Fluids* 59:64

Méheut M and Bailly D (2008) Drag-breakdown methods from wake measurements. *AIAA Journal* 46:847–862

Mohebbian A and Rival D (2012) Assessment of the derivative-moment transformation method for unsteady-load estimation. *Exp Fluids* 53:319–330

Neatby aYS H (2012) Towards reliable experimental drag measurements of an airfoil at low Reynolds numbers. in *42nd AIAA Fluid Dynamics Conference and Exhibit*. ASME, New Orleans, Louisiana

Noca F, Shiels D, and Jeon D (1999a) A comparison of methods for evaluating time-dependent fluid dynamic forces on bodies, using only velocity fields and their derivatives. *Journal of Fluids and Structures* 13:551–578

Noca F, Shiels D, and Jeon D (1999b) A comparison of methods for evaluating time-dependent fluid dynamic forces on bodies, using only velocity fields and their derivatives. *J Fluids Struct* 13:551–578

Poelma C, Dickson W, and Dickinson M (2006) Time-resolved reconstruction of the full velocity field around a dynamically-scaled flapping wing. *Exp Fluids* 41:213–225

Ragni D, van Oudheusden BW, and Scarano F (2012) 3D pressure imaging of an aircraft propeller blade-tip flow by phase-locked stereoscopic PIV. *Experiments in Fluids* 52:463–477

Rival D, Manejev R, and Tropea C (2010) Measurement of parallel blade-vortex interaction at low Reynolds numbers. *Exp Fluids* 49:89–99

Rival DE and van Oudheusden B (2017) Load-estimation techniques for unsteady incompressible flows.. *Exp Fluids* 58:20

Saffman P (1992) *Vortex Dynamics*. Cambridge University Press

Spedding G and Hedenström A (2009) PIV-based investigations of animal flight. *Exp Fluids* 46:749–763

Takahashi T (1997) On the decomposition of drag components from wake flow measurements. in *35th AIAA Aerospace Sciences Meeting and Exhibit*. pages 1–10. Reno, NV

Tronchin T, David L, and Farcy A (2015) Loads and pressure evaluation of the flow around a flapping wing from instantaneous 3D velocity measurements. *Experiments in Fluids* 56:1870

Unal M, Lin J, and Rockwell D (1997a) Force prediction by PIV imaging: a momentum-based approach. *J Fluids Struct* 11:965–971

Unal M, Lin J, and Rockwell D (1997b) Force prediction by PIV imaging: a momentum-based approach. *Journal of Fluids and Structures* pages 965–971

van Dam CP (1999) Recent experience with different methods of drag prediction.. *Prog Aerosp Sci* 35:751–798

van Oudheusden B (2013) PIV-based pressure measurement. *Measurement Science and Technology* 24:032001

van Oudheusden B, Scarano F, and Casimiri E (2006) Non-intrusive load characterization of an airfoil using PIV. *Experiments in Fluids* 40:988–992

van Oudheusden B, Scarano F, Roosenboom E, Casimiri E, and Souverein L (2007) Evaluation of integral forces and pressure fields from planar velocimetry data for incompressible and compressible flows. *Experiments in Fluids* 43:153–162

Villegas A and Diez F (2014) Evaluation of unsteady pressure fields and forces in rotating airfoils from time-resolved PIV. *Exp Fluids* 55:1697

Violato D, Moore P, and Scarano F (2011) Lagrangian and Eulerian pressure field evaluation of rod-airfoil flow from time-resolved tomographic PIV. *Experiments in Fluids* 50:1057–1070

Wu J, Ma H, and Zhou J (2006) *Vorticity and Vortex Dynamics*. Springer

Wu J, Pan Z, and Lu X (2005) Unsteady fluid-dynamic force solely in terms of control-surface integral. *Phys Fluids* 17:098102